WARSAW UNIVERSITY OF TECHNOLOGY Index 351733
FACULTY OF CIVIL ENGINEERING
COMMITTEE FOR CIVIL AND WATER ENGINEERING
POLISH ACADEMY OF SCIENCES ISSN 1230-2945
DOI: 10.24425/ace.2024.148919
ARCHIVES OF CIVIL ENGINEERING
Vol. LXX ISSUE 1 2024
pp. 405 –420

Research paper

The investigation on flexural performance of prestressed concrete-encased high strength steel beams

Jun Wang[1], Yurong Jiao[2], Menglin Cui[3], Wendong Yang[4], Xueqi Fang[5], Jun Yan[6]

Abstract: This paper reports an experimental on the flexural performance of prestressed concrete-encased high-strength steel beams (PCEHSSBs). To study the applicability of high-strength steel (HSS) in prestressed concrete-encased steel beams (PCESBs), one simply supported prestressed concrete-encased ordinary-strength steel beam (PCEOSSB) and eight simply supported PCEHSSBs were tested under a four-point bending load. The influence of steel strength grade, I-steel ratio, reinforcement ratio and stirrup ratio on the flexural performance of such members was investigated. The test results show that increasing the I-steel grade and I-steel ratio can significantly improve the bearing capacity of PCESB. Increasing the compressive reinforcement ratio of PCEHSSB can effectively improve its bearing capacity and ductility properties, making full use of the performance of HSS in composite beams. Increasing the hoop ratio has a small improvement on the load capacity of the test beams; setting up shear connectors can improve the ductile properties of the specimens although it does not lead to a significant increase in the load capacity of the combined beams. Then, combined with the test data, the comprehensive reinforcement index considering the location of reinforcement was proposed to evaluate the crack resistance of specimens. The relationship between the comprehensive reinforcement index and the crack resistance of specimens was given.

Keywords: high-strength steel, prestressed concrete-encased steel beam, flexural bearing capacity, crack resistance

[1]Prof., Northeast Forestry University, Faculty of Civil Engineering, Harbin 150000, China, e-mail: jun.w.619@nefu.edu.cn, ORCID: 0009-0003-2312-6108
[2]M.Sc., Northeast Forestry University, Faculty of Civil Engineering, Harbin 150000, China, e-mail: jyrongyx@163.com, ORCID: 0009-0000-2809-3059
[3]M.Sc., Northeast Forestry University, Faculty of Civil Engineering, Harbin 150000, China, e-mail: chch980115@google.com, ORCID: 0000-0001-9524-630X
[4]M.Sc., Northeast Forestry University, Faculty of Civil Engineering, Harbin 150000, China, e-mail: 19953808497@163.com, ORCID: 0009-0004-4117-4047
[5]M.Sc., Northeast Forestry University, Faculty of Civil Engineering, Harbin 150000, China, e-mail: fangxueqi@163.com, ORCID: 0009-0004-4632-4972
[6]PhD., Northeast Forestry University, Faculty of Civil Engineering, Harbin 150000, China, e-mail: yanjun92@163.com, ORCID: 0009-0008-2720-3461

1. Introduction

Concrete-encased steel composite constructions are currently employed extensively in high-rise buildings in several nations due to their higher bearing capacity than conventional concrete structures [1–8]. However, the bearing capacity of traditional concrete-encased ordinary-strength steel beams is no longer able to meet the demands of modern building structures owing to the rapid development of high-rise and large-span constructions. High-strength steel (HSS) not only has high yield strength (f_y > 460 MPa) but also weighs less, consumes less material, and reduces transport costs. HSS can be applied to meet the bearing capacity requirements of high-rise and large-span structures, further optimize the cross-sectional dimensions of concrete-encased ordinary-strength steel composite structures, and utilize less steel [9–11]. In addition, it has been shown that the incorporation of prestressing technology into concrete-encased steel beams can effectively inhibit the generation of cracks [7]. Therefore, HSS has broad application prospects in prestressed concrete-encased steel beams (PCESBs).

Recently, scholars from various countries have conducted several studies on concrete-encased HSS composite columns [11–14]. Related studies found that concrete crushed before the HSS yielded [11], preventing the full strength of steel from being utilized. However, the HSS yielded before the member reached its ultimate bearing capacity, which is due to the increasing configuration of the stirrups constrained the expansion of the concrete [13]. The calculation methods for the bearing capacity in the Chinese [15] and European [16] codes are too conservative for concrete-encased HSS composite columns under axial loads. A correction method based on the stirrup constraint principle is more consistent with the test results [13, 14]. Currently, for concrete-encased HSS beams, some studies related to finite element (FE) analysis are available [17, 18]. It was found that the use of HSS could increase the bearing capacity of the members, but there was a phenomenon of unyielding HSS in concrete-encased HSS beams. The accuracy of the analytical conclusions of the FE model remains to be experimentally verified, but fewer experimental studies have been reported on structures with concrete-encased HSS beams [10, 19–21]. Md. Imran Kabir [10] conducted flexural performance tests on Engineered Cementitious Composites and Lightweight Concrete (ECC-LWC). The results showed that HSS composite beams wrapped by ECC-LWC exhibited higher load carrying capacity and ductility properties compared to those wrapped by ordinary concrete.Zuqiang Liu [20] designed and fabricated six Q460 HSS ultra-high-performance concrete composite beams. The bending performance of these beams was studied using I-steel ratio, section location, and steel fiber volume as test parameters. The test results indicated suitable reinforcement damage in all specimens, with tensile reinforcement yielding and the lower flange of the section experiencing deformation before the concrete crushed in the compression zone. These studies excluded conventional stirrups and longitudinal reinforcement, had fewer parameters, and did not incorporate prestressing tendons, which hinders the advancement of HSS. which did not consider the effect of reinforcement on the yielding characteristics of H-beams and had no effective methods of controlling cracks.

For the HSS to be more effectively used in combination with PCESBs, the bottom flange of HSS must yield before the concrete is crushed and the crack development should be better controlled. To this end, this study carried out tests on the flexural performance of nine simply

supported PCESBs under four-point bending loads, thereby investigating the effect of the I-steel grade, steel to concrete ratio, longitudinal reinforcement ratio, and stirrup ratio on flexural performance.

2. Experimental study

2.1. Test specimens

Nine specimens were designed for this study. The length of the beams was 3100 mm, and the cross-section was 250×300 mm. The specimens used HRB400 grade longitudinal reinforcement and HPB300 grade stirrup reinforcement with a stirrup diameter of 8 mm, and welded H-beams were used for the section steel. The unbonded prestressed wires were of 1860 grade ($f_{\text{ptk}} = 1860$ N/mm^2), and the prestressed tendon tension adopted the unbonded post-tension method, with a nominal diameter of 15.2 mm. The tensioning control stress $\sigma_{\text{con}} = 0.65 f_{\text{ptk}}$. The concrete cover depth was 20 mm. Table 1 lists the design parameters and the actual effective prestressing of the tested beams. The test piece numbers and descriptions are presented in Fig. 1. The test parameters were the I-steel grade, steel to concrete ratio, longitudinal reinforcement ratio, stirrup ratio, and shear connectors. The geometry and construction of the specimens are shown in Fig. 2. Pins of 16×40 mm were selected as the shear connectors to be welded to the top flange of the steel, with an arrangement in accordance with that provided in the literature [22]. The exact position is shown in Fig. 3.

Table 1. Key parameters of specimens

Specimen	I-steel shape (mm) $b_f \times h \times t_1 \times t_2$	I-steel grade	I-steel ratio (%)	Tensile bars	Compression bars	Stirrup ratio (%)	Bolt	Effective prestress (MPa)
$B_1Q_3S_3R_1H_4C_1$	$100 \times 150 \times 8 \times 5$	Q355	3.03%	2ϕ14	3ϕ20	0.4	With	1150
$B_2Q_5S_3R_1H_4C_1$	$100 \times 150 \times 8 \times 5$	Q550	3.03%	2ϕ14	3ϕ20	0.4	With	1211
$B_3Q_6S_2R_1H_4C_1$	$100 \times 150 \times 5 \times 5$	Q690	2.27%	2ϕ14	3ϕ20	0.4	With	1207
$B_4Q_6S_3R_1H_4C_0$	$100 \times 150 \times 8 \times 5$	Q690	3.03%	2ϕ14	3ϕ20	0.4	With-out	1166
$B_5Q_6S_3R_1H_4C_1$	$100 \times 150 \times 8 \times 5$	Q690	3.03%	2ϕ14	3ϕ20	0.4	With	1178
$B_6Q_6S_3R_2H_4C_1$	$100 \times 150 \times 8 \times 5$	Q690	3.03%	3ϕ14	4ϕ20	0.4	With	1260
$B_7Q_6S_3R_0H_4C_1$	$100 \times 150 \times 8 \times 5$	Q690	3.03%	2ϕ14	2ϕ18	0.4	With	1181
$B_8Q_6S_3R_1H_8C_0$	$100 \times 150 \times 8 \times 5$	Q690	3.03%	2ϕ14	3ϕ20	0.81	With-out	1133
$B_9Q_6S_4R_1H_4C_1$	$100 \times 150 \times 10 \times 10$	Q690	4.4%	2ϕ14	3ϕ20	0.4	With	1125

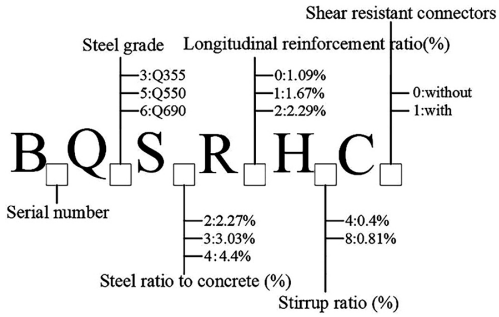

Fig. 1. Labeling rule of specimens

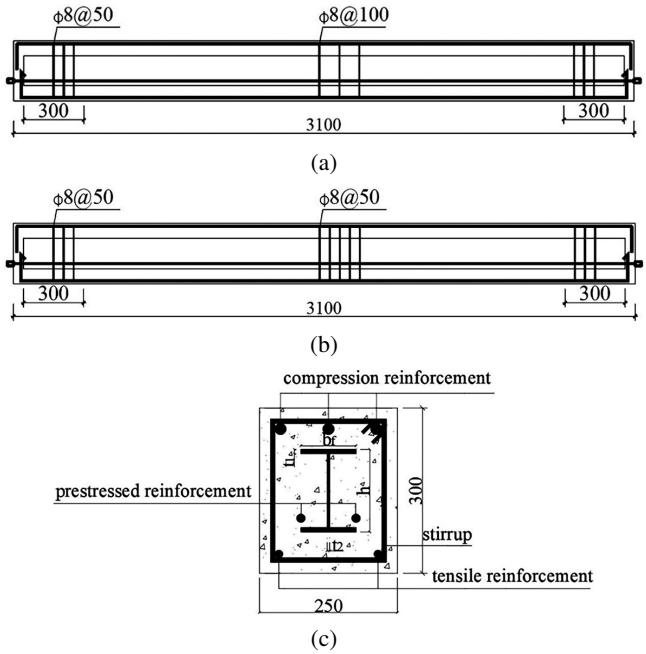

Fig. 2. Geometry and construction of specimens: a) The shape and reinforcement of B-1 2 3 4 5 6 7 9, b) The shape and reinforcement of B-8, c) Cross-section of the specimens (mm)

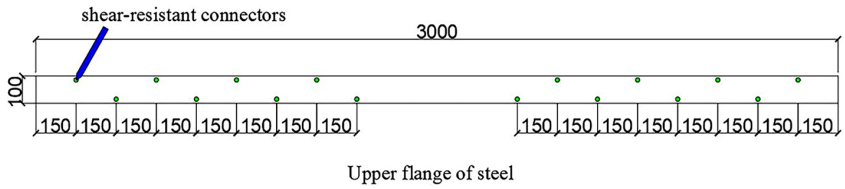

Fig. 3. Arrangement of the shear-resistant connectors

2.2. Material properties

According to the specifications of Chinese standard (GB/T 228.1-2021) [23], standard mechanical property testing was conducted. The mechanical properties of the steel plates used in the welded H-beams, longitudinal reinforcement, and stirrups are listed in Table 2.

C50 concrete was chosen for the specimens, and after the preparation work was completed, all specimens were poured simultaneously. The mechanical properties of the concrete specimens were maintained by curing under the same conditions, and the specimens were tested according to the standard for test methods of concrete structures (GB/T50152-2012) [24]. The average cubic compressive strength of the nine concrete cube specimens ($150 \times 150 \times 150$ mm) was 55.3 MPa.

Table 2. Mechanical properties of steel

Grade	Thicknesses (Diameters) (mm)	Yield strength f_y (MPa)	Ultimate strength f_w (MPa)	Elongation at break δ (%)
Q355	5	397	527	42.9
Q355	8	391	540	22.6
Q550	5	626	713	26.5
Q550	8	633	756	19.4
Q690	5	740	819	22.6
Q690	8	787	845	17.7
Q690	10	690	766	21.7
prestressed wire	15.2	1820	1910	20.5
HPB300	8	358	537	23.9
HRB400	14	453	591	25.6
HRB400	18	415	586	28.7
HRB400	20	433	566	29.5

Note: Q – for I-shape, HRB – for longitudinal bars, HPB – for transverse bars (stirrups)

2.3. Loading method and measurement point arrangement

The length of the bending-shear section of the specimen was 1000 mm, and the length of the pure bending section in the spanwise direction was 800 mm. The test was performed using a stepped loading method; the loading apparatus is shown in Fig. 4. Before loading, the specimen was preloaded, and the apparatus was commissioned. When loading to 80% of the cracking load estimate, the load was applied at approximately 5% of the cracking load estimate until the first crack appeared and resumed normal loading. Subsequently, normal loading was

applied, and the magnitude of the load at each step was 10% of the estimated ultimate load. When the maximum crack width of the beam reached 0.15 mm, the load at each step was approximately 5% of the cracking load estimate until the maximum crack width exceeded 0.2 mm. When the loading reached 80% of the estimated ultimate load of the tested beam, subsequent loads were increased at a rate of 5% per step until the specimens were damaged (i.e., until the ultimate load of the beams was reached). The damage was marked by the failure of the concrete in the compressive zone and the beginning of load reduction on the beams. After the ultimate load was reached, the loading method was changed to a displacement-controlled loading at a loading speed of 2 mm/min. The loading was terminated when the load on the tested beam reached 0.85 times the beam's ultimate bearing capacity.

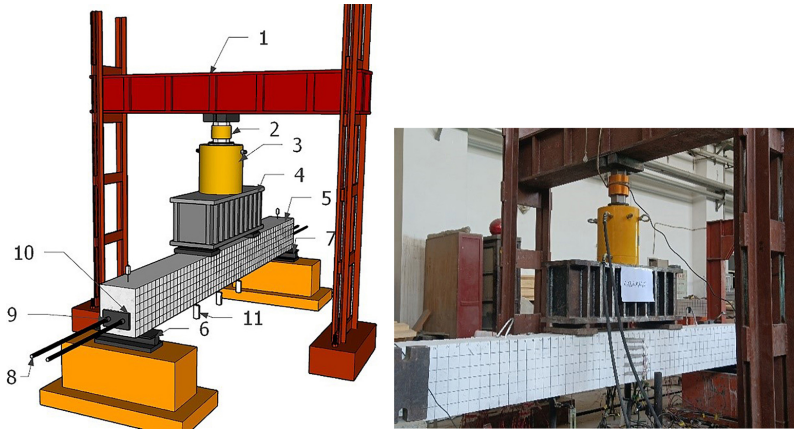

Fig. 4. Test setup and instrumentation: 1 – counterweight frame, 2 – pressure sensor, 3 – jack, 4 – distribution beam, 5 – specimen, 6 – fixed hinge support, 7 – sliding hinge support, 8 – steel strands, 9 – anchorage, 10 – steel plate, 11 – displacement meter

The load was applied using a jack via a distribution beam, and the magnitude of the applied load was gauged using a pressure transducer. To measure the displacement of the beams, five displacement gauges were placed at the support, bottom of the loading point in the span, and bottom of the beams. Strain gauges were placed at regular intervals on the surfaces of the longitudinal reinforcement and steel within the length of the pure bending section to measure the strain change throughout the test. The arrangement of strain gauges on the longitudinal reinforcement and steel is shown in Fig. 5.

The magnitude of the preload was measured by means of a 25t through-center transducer, as shown in Fig. 6. The tensioning control stress of the prestressing tendons, σ_{con}, was taken as 0.65 f_{ptk}. Each unbonded prestressing tendon was over-tensioned to $1.05\sigma_{\text{con}}$ and held for 2 minutes and then depressurized. Observing the load change on the sensor during the load holding process, and take the measure of re-tensioning for large loss of prestressing force, and the control stress of re-tensioning is con.

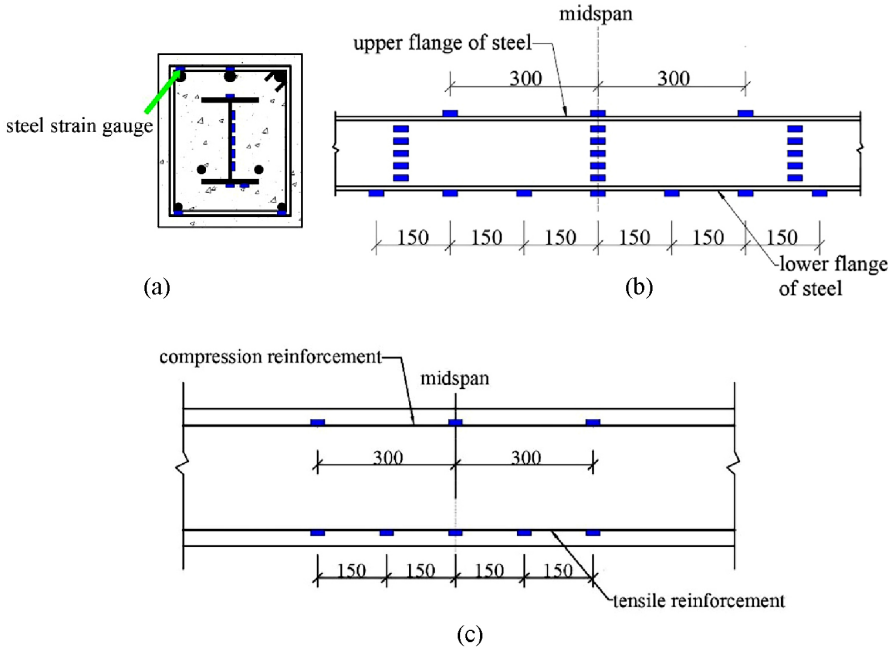

Fig. 5. Arrangement of strain gauge positions for: a) Cross-sectional view, b) Steel, c) Longitudinal bars

Fig. 6. Prestressing tendon tensioning: a) Holding a load, b) After tensioning

3. Test results and analysis

3.1. Description of test phenomenon

The damage modes of all tested beams were bending damage. Due to the presence of prestressing tendons, the tested beams showed some reverse arching before loading. According to the test phenomena, the test processes of beams B1–B9 can be divided into four stages.

Stage 1: Before cracking of tested beams. At this time, the concrete in the tensile zone was not cracked, the strains on the steel and concrete were small, the tested specimens were in the elastic stage, and the reverse arch of the tested beams gradually disappeared.

Stage 2: The tested beams at the bottom flange of the steel yield. When the load was loaded to approximately 0.25 times ultimate load ($0.25P_u^t$), the tested beams cracked and vertical cracks appeared in the span of the tested beams. According to the data of the strain gauges, when loaded to (0.49 ~ 0.6) P_u^t, the tensile reinforcement was the first to yield. As the load continued to increase, the steel bottom flange began to yield. At (0.74 ~ 0.91) P_u^t, the bottom flange of the steel fully yielded, at which time the slopes of the Load–deflection curves of the specimen began to decrease, and the tested beams entered the yielding stage.

Stage 3: Reaching the ultimate load. After the bottom flange of the steel yielded, the tested beams entered the elastic-plastic phase where the beam deflection increased, the strands were further tensed, and cracks developed rapidly upward. The web started to yield as the load increased, the yield region of the section steel stretched upward, and the load on the tested beams continued to increase. The tested beams reached the ultimate bearing capacity when the concrete in the compressive zone was crushed.

Stage 4: After reaching the ultimate load. After the beams reached the ultimate bearing capacity, the load on the tested beams did not rapidly decrease. Owing to the presence of built-in steel [6], the tested beams exhibited a good load-holding capacity after the concrete was crushed, at which time the load started to decrease slowly. Thereafter, the deflection of the tested beams continued to increase, and the loading stopped after dropping to $0.85P_u^t$.

After unloading, the prestressing strands contracted rapidly and the deflection of the tested beam recovered rapidly, showing good crack closure performance, which reflected the effect of applied prestressing. Fig. 7 showed a comparison of the parts of the tested beams after damage. The top concrete of all the tested beams was crushed after the bottom flange of the steel yielded, and the strength of the steel was fully utilized.

(a)

(b)

(c)

Fig. 7. The parts of the tested beams after damage: a) Tested beam $B_5Q_6S_3R_1H_4C_1$, b) Tested beam $B_7Q_6S_3R_0H_4C_1$, c) Tested beam $B_8Q_6S_3R_1H_8C_0$

3.2. Strain distribution of cross-section in the span

The strain distribution plotted along the height of the steel is shown in Fig. 8.

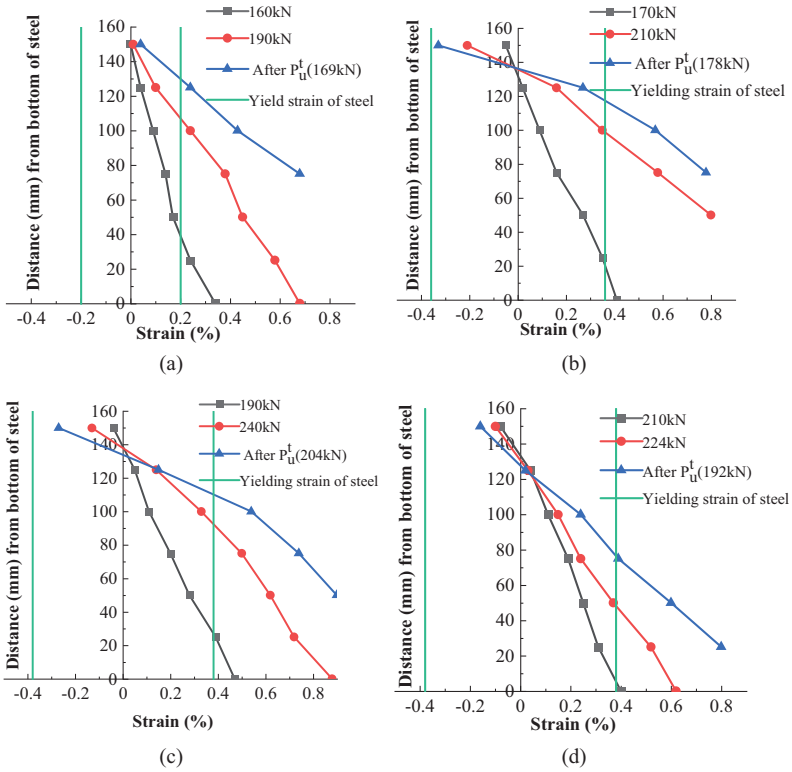

Fig. 8. Strain distribution along the depth of the beams: a) B1, b) B3, c) B5, d) B7

The figure shows that (1) the strain in the span along the height direction of the beams showed a good linear relationship, and the assumption of a flat section was met. (2) The bottom flange of each steel beam fully yielded in tension, and the steel web yielded to a high height, fully utilizing the steel's tensile strength. (3) The beam with a lower I-steel ratio (B3, compared with B5) and the beam with more compression reinforcement (B5, compared with B7) had higher utilization of steel strength.

3.3. Load bearing capacity and Ductility behaviour

The yield loads (P_y^t) were determined by the Graphical Method of the literature [25], as shown in Fig. 9. The yield loads (P_y^t) and ultimate loads (P_u^t) of the specimens and the corresponding displacements are shown in Table 3. The displacement ductility coefficient expressed as the ratio $\Delta_{\max}/\Delta_y$ of the displacement at $0.85P_u^t$ (after ultimate loads) to the displacement at P_y^t is shown in Table 3.

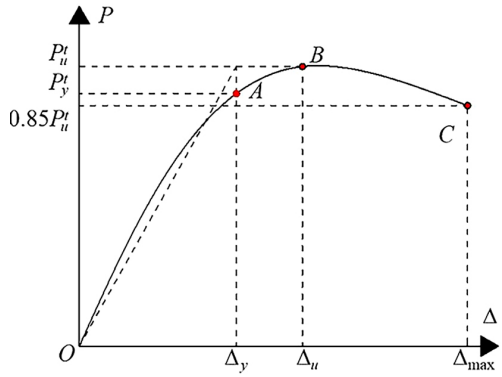

Fig. 9. Graphical Method

Table 3. Loads and displacement of specimens at different stages

Specimen	P_y^t (kN)	Displacement Δ_y (mm)	P_u^t (kN)	Displacement Δ_u (mm)	Δ_{max} (mm)	Ductility coefficient Δ_{max}/Δ_y
$B_1Q_3S_3R_1H_4C_1$	163	20.8	190	39.2	68.3	3.28
$B_2Q_5S_3R_1H_4C_1$	176	19.6	223	40.1	70.5	3.59
$B_3Q_6S_2R_1H_4C_1$	170	20.1	210	46.7	74.7	3.72
$B_4Q_6S_3R_1H_4C_0$	200	25.2	237	40.6	74	2.94
$B_5Q_6S_3R_1H_4C_1$	195	21.3	240	41.4	76.4	3.59
$B_6Q_6S_3R_2H_4C_1$	201	21.8	264	44.3	60.1	2.76
$B_7Q_6S_3R_0H_4C_1$	205	26.5	224	35.9	72.3	2.73
$B_8Q_6S_3R_1H_8C_0$	205	26.7	244	45.7	78.2	2.93
$B_9Q_6S_4R_1H_4C_1$	228	22.5	277	46.4	62.8	2.79

3.3.1. Effect of i-steel grade and I-steel ratio

Figures 10 and 11 show the load-deflection curves of beams with different I-steel grades and ratios, respectively. When the I-steel grade was increased from Q355 to Q550 and Q690, the bearing capacity of the tested beams was increased by 17.4% and 26.3%, respectively. Compared to the specimens with an I-steel ratio of 2.27%, the bearing capacities of the beams with I-steel ratios of 3.03% and 4.4% increased by 14.3% and 31.9%, respectively. The ductility coefficients of the specimens decreased from 3.72 to 3.59 and 2.79 when the I-steel ratio increased. These results indicate that increasing both the I-steel grade and I-steel ratio can greatly increase the flexural strength of the tested beams, but the increase in I-steel ratio decreases the ductility coefficient of prestressed concrete-encased high-strength steel beams (PCEHSSBs).

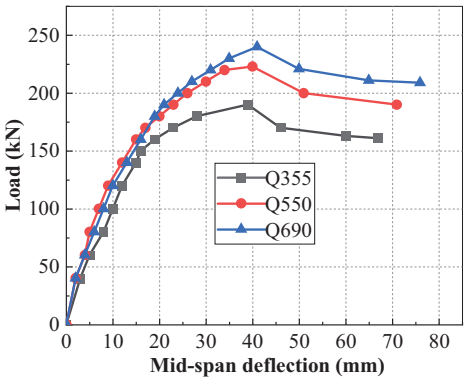

Fig. 10. Load-deflection curves for different I-steel grades

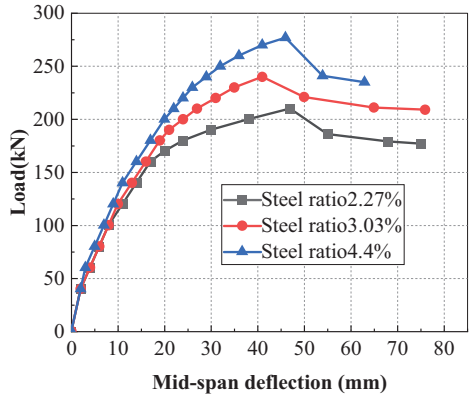

Fig. 11. Load-deflection curves for different I-steel ratios

3.3.2. Effect of longitudinal reinforcement ratio

The load-deflection curves for beams B7, B5, and B6 with longitudinal reinforcement ratios of 1.09%, 1.67%, and 2.29%, respectively, are shown in Fig. 12. When the ratio of longitudinal reinforcement was increased from 1.09% to 1.67% and 2.29%, the bearing capacity of the members was increased by 7.1% and 17.9%, respectively. When the ratio of compression reinforcement was increased from 0.68% to 1.3%, the displacement ductility coefficient of the specimen was increased by 31.5%. The yield load of beam B7 is 0.92 times the ultimate load, while the yield load of beam B5 with only additional compression reinforcement is 0.81 times the ultimate load. Beam B5 had a higher strength utilization of steel than B7. This is because increasing the configuration of the compression reinforcement enhanced the compressive capacity of the beam in the compressive zone and making better use of the strength of the HSSS while enhancing the bearing capacity of the beams.

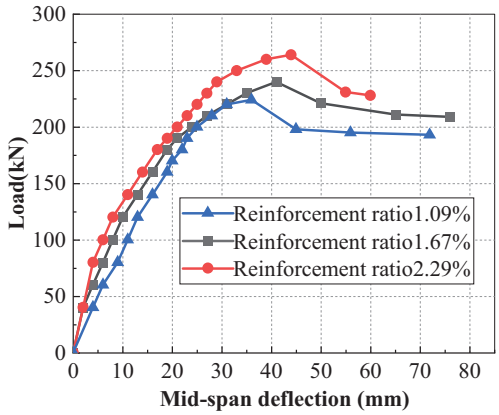

Fig. 12. Load-deflection curves for different reinforcement ratios

3.3.3. Effect of stirrup ratio and shear connectors

Figure 13 shows the load-deflection curves of beams B4, B5, and B8. Comparing the ultimate loads of beams B4 and B8, it was found that when the stirrup ratio continued to increase to 0.8% from 0.4%, the bearing capacity increased by the smaller amount of 3%. The ultimate loads of beams B4 and B5 are compared in Table 3, which shows that the natural bonding action between the HSS and concrete can ensure the reliable transmission of shear force and setting shear connectors can improve the displacement ductility coefficient of tested beams.

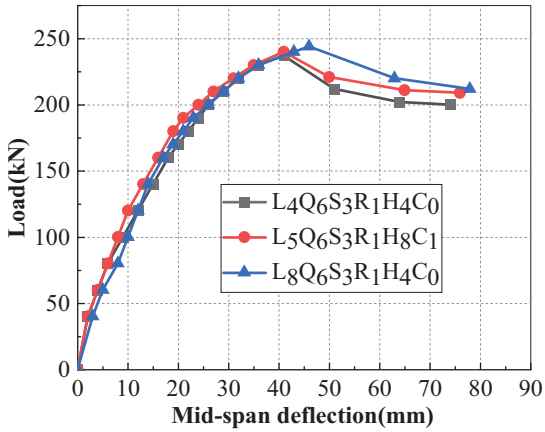

Fig. 13. Load-deflection curves of B4, B5 and B8

3.4. Cracking performance

Table 4 shows the cracking performance of different specimens, and Fig. 14 demonstrates the crack width of the tested beams under different loading conditions. It can be seen that as the I-steel grade increases, the number of cracks increases and the growth rate of crack width increases after the maximum crack width exceeds 0.2 mm. According to the Code for design of prestressed concrete structures [26] (JGJ 369-2016), the maximum allowable crack width of PCESSBs is 0.2mm. In this paper, the bending moment when the maximum crack width reaches 0.2 mm is defined as M_C and the ultimate bending moment of the member is M_U. The value of M_C/M_U reflects the crack resistance of the member, and the M_C/M_U values of each specimen are shown in Table 4. As shown in Table 4, it can be seen that the crack resistance of PCEHSSBs is better than that of prestressed concrete-encased ordinary-strength steel beams (PCEOSSBs), and increasing both the I-steel ratio and reinforcement ratio can improve the crack resistance of the members. Referring to the study of prestressed concrete members [27,28], the comprehensive reinforcement index ρ is used to describe the reinforcement of the members in this paper, and the formula for calculating the comprehensive reinforcement index ρ is shown in equations (3.1)–(3.5), and the calculation results are shown in Table 4.

Table 4. Cracking performance of beams

Specimen	Cracking load (kN·m)	Number of cracks	Maximum crack height (mm)	ρ	M_C/M_U
$B_1Q_3S_3R_1H_4C_1$	50	17	247	0.262	0.611
$B_2Q_5S_3R_1H_4C_1$	45	19	241	0.345	0.661
$B_3Q_6S_2R_1H_4C_1$	52.5	24	252	0.323	0.655
$B_4Q_6S_3R_1H_4C_0$	52.5	23	260	0.397	0.675
$B_5Q_6S_3R_1H_4C_1$	55	20	203	0.398	0.677
$B_6Q_6S_3R_2H_4C_1$	55	23	250	0.417	0.682
$B_7Q_6S_3R_0H_4C_1$	47.5	24	249	0.4	0.676
$B_8Q_6S_3R_1H_8C_0$	50	21	247	0.395	0.677
$B_9Q_6S_4R_1H_4C_1$	52.5	22	231	0.487	0.693

$$\rho = \frac{\alpha_s f_y A_s + \alpha_p f_p A_p + \alpha_a f_a A_a + \alpha_{\mathrm{w}} f_{aw} A_{aw}}{f_{\mathrm{c}} bh} \tag{3.1}$$

$$\alpha_s = \frac{h - a_s}{h} \tag{3.2}$$

$$\alpha_p = \frac{h - a_p}{h} \tag{3.3}$$

$$\alpha_a = \frac{h - a_a}{h} \tag{3.4}$$

$$\alpha_{\mathrm{w}} = \frac{h - a_{aw}}{h} \tag{3.5}$$

where: f_y, f_p, f_a, f_{aw} – the yield strength of the tensile reinforcement, steel strands, bottom flange of steel, web of steel and steel strands respectively; a_y, a_p, a_a, a_{aw} – the distance from the center of the tensile reinforcement, steel strands, bottom flange of steel, and web of steel respectively, to the edge of the compressive zone; A_s, A_p, A_a,A_{aw} – are the cross-sectional areas of the tensile reinforcement, steel strands, bottom flange of steel, and web of steel respectively.

The plot of ρ and M_C/M_U is given in Fig. 15, and it can be found that M_C/M_U tends to increase nonlinearly with the increase of ρ, and the increase amount decreases gradually.

M_C is the bending moment when the maximum crack width reached 0.2 mm, M_U is ultimate bending moment, ρ is comprehensive reinforcement index.

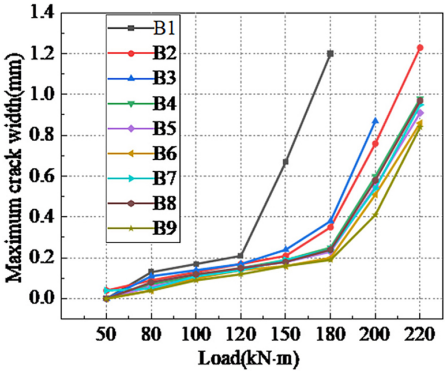

Fig. 14. Crack widths under different loads

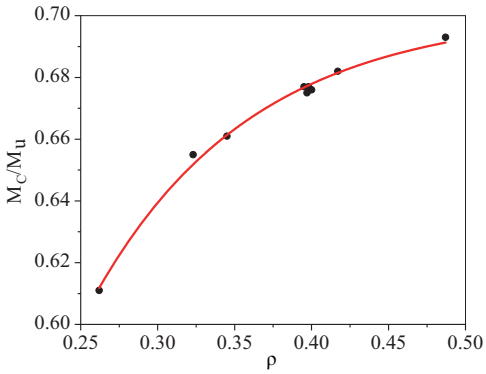

Fig. 15. Relationship between ρ and M_C/M_U

4. Summary

This study verified the applicability of HSS on PCESBs. Based on the results obtained from the tests and FE analysis, the following conclusions can be drawn:

1. The HSS could significantly improve the flexural bearing capacity of PCESBs, and compared with Q355 PCESB, the flexural bearing capacities of Q550 and Q690 PCESBs were increased by 17.4% and 26.3%, respectively. The flexural bearing capacity of PCEHSSB with I-steel ratios of 3.03% and 4.4% increased by 14.3% and 31.9%, respectively, compared with that of the specimen with a ratio of 2.27%. When the reinforcement ratio was increased from 1.09% to 1.67% and 2.29%, the bearing capacity of the members was increased by 7.1% and 17.9%, respectively.
2. The bearing capacity of the beam, ductility of the specimen, and utilization of the strength of the steel could all be improved by increasing the configuration of the compression reinforcement. The bearing capacity of the tested beam improved less when the stirrup ratio increased. The provision of shear connectors did not result in a significant increase in the bearing capacity of the tested beam; however, it improved the displacement ductility coefficient of the specimen.
3. The comprehensive reinforcement index ρ was proposed to evaluate the cracking resistance of the tested beams, and the analysis showed that ρ was positively correlated with the cracking resistance of the beams, for which a relationship curve was fitted.

References

[1] L. Binglin and J. Liew, "Axial-moment interaction of high strength concrete encased steel composite columns: Experimental investigation", *Journal of Constructional Steel Research*, vol. 175, art. no. 106370, 2020, doi: 10.1016/j.jcsr.2020.106370.

[2] Z. WeiQing, M. Gang, and J. JinQing, "Experimental studies on axial load performance of high-strength concrete short columns", *Proceedings of the Institution of Civil Engineers – Structures and Buildings*, vol. 167, no. 9, pp. 509–519, 2014, doi: 10.1680/stbu.13.00027.

[3] B. Lai, J.Y.R. Liew, et al., "Assessment of high-strength concrete encased steel composite columns subject to axial compression", *Journal of Constructional Steel Research*, vol. 164, 2020, doi: 10.1016/j.jcsr.2019.105765.

[4] K. Wu, F. Chen, C. Chen, et al., "Load-transfer mechanism and bond-stress components in steel and steel fiber-reinforced concrete structure", *Journal of Structural Engineering*, vol. 145, no. 12, 2019, doi: 10.1061/(asce)st.1943-541x.0002441.

[5] T. Qinglin, N. Ben, G. Yongying, et al., "Experimental and theoretical study on flexural behavior of high strength concrete encased steel beams with steel fibers", *Structures*, vol. 41, pp. 1359–1368, 2022, doi: 10.1016/j.istruc.2022.05.073.

[6] J. Jinqing, M. Gang, and Z. Weiqing, "Experimental study and bearing capacity analysis of prestressed steel ultra-high strength concrete composite beams", *Journal of Architectural Structure*, vol. 35, no. 9, pp. 1–10, 2014, doi: 10.14006/j.jzjgxb.2014.09.001.

[7] F. Chuanguo, L. Yuying, and L. Shuting, "Experimental study on flexural behaviour of prestressed steel-concrete beam with simple support", *Journal of Architectural Structure*, no. 3, pp. 62–73, 2007, doi: 10.14006/j.jzjgxb.2007.03.009.

[8] M. Szadkowska and E. Szmigiera, "Bond between steel and SCC in completely concrete encased HEA 160 I-section columns", *Archives of Civil Engineering*, vol. 68, no. 3, pp. 125–137, 2022, doi: 10.24425/ace.2022.141877.

[9] H. Bin and Z. Wen-Fu, "Overall buckling performance of high strength steel welded I-sections under combined axial compression and bending", *Archives of Civil Engineering*, vol. 68, no. 3, pp. 369–384, 2022, doi: 10.24425/ace.2022.141891.

[10] M. Kabir, C. Lee, et al., "Flexural behaviour of ECC-LWC encased slender high strength steel composite beams", *Journal of Constructional Steel Research*, vol. 173, 2020, doi: 10.1016/j.jcsr.2020.106253.

[11] K. Chang-Soo, P. Hong-Gun, and C. Kyung-Soo, "Eccentric Axial Load Testing for Concrete-Encased Steel Columns Using 800 MPa Steel and 100 MPa Concrete", *Journal of Structural Engineering*, vol. 138, no. 8, pp. 1019–1031, 2012, doi: 10.1061/(asce)st.1943-541x.0000533.

[12] B. Lai and J. Liew, "Design and testing of concrete encased steel ncomposite beam-columns with C90 concrete and S690 steel section", *Engineering Structures*, vol. 220, art. no. 110995, 2020, doi: 10.1016/j.engstruct.2020.110995.

[13] W. Jun, S. Yu, et al., "Study on axial compression performance of high-strength H-shaped steel concrete composite column", *Journal of Building Structures*, vol. 43, pp. 191–200, 2022, doi: 10.14006/j.jzjgxb.2021.0086.

[14] J. Wang, Y. Duan, et al., "Analysis and Modification of Methods for Calculating Axial Load Capacity of High-Strength Steel-Reinforced Concrete Composite Columns", *Materials (Basel)*, vol. 14, no. 22, 2021, doi: 10.3390/ma14226860.

[15] JGJ138-2016 Code for Design of Composite Structures. Beijing, China: Architecture and Building Press, 2016.

[16] EN 1994-1-1:2004 Eurocode 4. Design of Composite Steel and Concrete Structures Part 1-1: General Rules for Buildings. Brussels, Belgium: European Committee for Standardization, 2004.

[17] L. BingLin, Y. Lifu, and X. MingXiang, "Numerical simulation and data-driven analysis on the flexural performance of steel reinforcednconcrete composite members", *Engineering Structures*, vol. 247, 2021, doi: 10.1016/j.engstruct.2021.113200.

[18] M. Rana, C. Lee, et al., "Flexural behaviour of steel composite beams encased by engineered cementitious composites", *Journal of Constructional Steel Research*, vol. 143, pp. 279–290, 2018, doi: 10.1016/j.jcsr.2018.01.004.

[19] L. Hao, "Study on the force performance of high-strength steel and concrete flexural members", M.A. thesis, Xi'an University of Architecture and Technology, China, 2005.

[20] L. Zuqiang, R. Bengyou, and X. Jianyang, "Experimental study and finite element analysis on flexural performance of high-strength steel reinforced ultra-high performance concrete beam", *Engineering Mechanics*, vol. 40, no. 4, pp. 1–15, 2023, doi: 10.6052/j.issn.1000-4750.2021.10.0765.

[21] M. Kabir, C.K. Lee, et al., "Strength enhancement of high strength steel beams by engineered cementitious composites encasement", *Engineering Structures*, vol. 207, 2020, doi: 10.1016/j.engstruct.2020.110288.

[22] Z. Bo, "Experimental study on flexural behaviour of unbonded prestressed steel concrete beams", M.A. thesis, Hunan University, China, 2013.

[23] GB/T228.1-2021 Metallic materials – Tensile testing – Part 1: Method of test at room temperature. Beijing, China: Architecture and Building Press, 2021.

[24] GB/T50152-2012 Standard for test method of concrete structures. Beijing, China: Architecture and Building Press, 2012.

[25] X. Jixiang, W. ShuaiLin, et al., "Seismic performance of shear energy dissipation beams in D-shaped eccentrically braced steel frames", *Journal of Constructional Steel Research*, vol. 180, 2021, doi: 10.1016/j.jcsr.2021.106584.

[26] JGJ 369-2016 Code for design of prestressed concrete structures. Beijing, China: Architecture and Building Press, 2016.

[27] L. Zhang, "Experimental study of ductility of prestressed high-strength concrete beams", *Engineering Mechanics*, vol. 22, no. 3, pp. 166–171, 2005.

[28] L. Xiaoyong, C. Yuecke, and D. Pengqi, "Experimental study on fatigue properties of unbonded partially prestressed concrete beams", *Journal of Architectural Structure*, vol. 28, pp. 98–104, 2007

Received: 2023-03-30, Revised: 2023-09-12